International Journal of Wireless Information Networks
https://doi.org/10.1007/s10776-019-00426-x

3D Localization Performance Evaluation using IMU/TOA Fusion Methods

Cheng Xu[1,2,3] · Jie He[1,2,3] · Xiaotong Zhang[1,2,3] · Shihong Duan[1,2,3] · Cui Yao[1,2,3]

Received: 16 December 2018 / Accepted: 2 April 2019

Abstract
Location is a basic property of an object. In the last decades, much attention has been paid to the precise localization and performance evaluation in wireless sensor networks. Time-of-arrival (TOA) and inertial measurement unit (IMU) based localization methods have been drawing attentions due to their advantageous performance. However, TOA suffers from the multipath effect and IMU from error accumulation problem, which have limited their application prospects. Thus, the fusion of these two methods becomes necessary. Besides, in existing literatures, when estimating the positioning accuracy, it is generally assumed that the position of base station is error-free, which is not so consistent with reality. Thus, for the purpose of achieving high precision positioning in practical conditions, we modeled the anchor position error, IMU error, and TOA error, respectively. Based on these models, CRLB and PCRLB in 3-D environment are deduced to evaluate positioning accuracy in both spatial and temporal level. Finally, CRLB and PCRLB are considered when different base station topologies are used, as well as compared with commonly used localization algorithms. Experimental results show that the impacts of anchor position error on positioning results cannot be ignored. CRLB and PCRLB can be used as benchmarks based on IMU/TOA fusion positioning systems and as reference lower bounds for performance improvement of localization algorithms.

Keywords Inertial measurement unit (IMU) · Time of arrival (TOA) · Performance · Cramér–Rao lower bound (CRLB)

1 Introduction

Wireless sensor network (WSN) is composed of a large number of stationary or moving sensors in a self-organizing and multi-hop manner to cooperatively perceive, collect, process and transmit information of perceived objects in a network coverage area through wireless communication. It can be applied in many fields, such as military [1], emergency [2], industrial [3] and etc., to monitor various data information. Many of these information need to be associated with corresponding targets' location, so the acquisition of node location information in WSN is very important [4].

Global positioning system (GPS) is an all-around, all-weather, full-time, high-precision satellite navigation system that provides global users with low-cost, high-precision information [5]. However, the effectiveness of GPS is limited in harsh environment such as dense building areas, where GPS signals cannot penetrate most of the obstacles [6]. New positioning technology is therefore needed to meet the demand for precise positioning in these conditions. Time-of-Arrival (TOA) positioning can provide accurate distance measurement in harsh environment because of its accurate delay resolution and robustness. It is widely used in wireless sensor network positioning systems [6, 7]. However, TOA ranging method is susceptible to multipath effects and the relative positional relationship between nodes [6]. In recent years, inertial navigation system (INS) as an auxiliary positioning method can compensate TOA's multipath effects and geometric topology problems. Inertial measurement units (IMU) such as

✉ Cheng Xu
xucheng19880202@foxmail.com

1 School of Computer and Communication Engineering, University of Science and Technology Beijing, Beijing 100083, China

2 Beijing Advanced Innovation Center for Materials Genome Engineering, University of Science and Technology Beijing, Beijing 100083, China

3 Beijing Key Laboratory of Knowledge Engineering for Materials Science, Beijing 100083, China

Published online: 08 April 2019

accelerometers, gyroscopes, magnetometers, etc., can provide a series of continuous inertial information to improve positioning accuracy [8, 9]. However, inertial sensors may inevitably throw off errors that accumulate over time [10, 11]. The accumulative and drift error is the biggest challenge faced by IMU-based localization systems.

Fusion filtering methods, such as Kalman [12] and particle filtering [14], are widely used in IMU/TOA fusion-based localization applications. Zhao et al. [12] proposed a Kalman/UFIR filtering method for state estimation with uncertain parameters and noise statistics. Briese et al. [13] presented an adapting covariance Kalman filter based on sensor fusion of UWB localization and inertial measurements. Since both sensor results were separately used in the Kalman filter, no registration between the implemented sensors was needed. Kim et al. [14] proposed a fusion algorithm based on a particle filter using vertical and road intensity information for robust vehicle localization in a large scale urban area.

In regional positioning systems, the network usually consists of two types of nodes: anchor nodes (i.e., base stations) and target nodes [6]. It is generally assumed that the anchor position is known and there is no error [16, 17]. The location of target nodes are unknown. Each node is equipped with a RF transceiver, and we can get the wireless signal parameters related to distances or angles when the target node performs radio communication with base stations [18, 19, 22, 23]. The location of the target nodes are uncertain due to the influence of random factors, such as noise, fading, multipath, and non-line-of-sight propagation, which ultimately affect the positioning accuracy. Thus, how to evaluate the performance of the algorithm accurately is also the focus of the localization problem in WSN [13]. Cramér–Rao lower bound (CRLB) defines the theoretical lower bound of any unbiased estimator variance and is used as a general criterion for evaluating the performance of a positioning system [24–26]. However, CRLB only focuses on the influence of the relationship between relative positions in spatial state on the accuracy of positioning targets. CRLB neglects the time information, and cannot meet the requirements of the time evaluation in the positioning system. The posterior Cramér–Rao lower bound (PCRLB) considers the time-domain information [20, 27] and can be used as another criterion for the performance evaluation of positioning systems.

Thus, based on above mentioned considerations, for the purpose of achieving high precision positioning in practical conditions, we modeled the anchor position error, IMU error, and TOA error, respectively. Based on these models, CRLB and PCRLB in 3-D environment are deduced to evaluate positioning accuracy in both spatial and temporal level. The main contributions of this paper are as follows:

- IMU/TOA fusion based localization algorithm for WSN is presented, which can compensate the TOA multi-path effect and IMU error accumulation problem;
- Comprehensively, both spatial and temporal performance are evaluated in 3-D scenarios, with considering various factors in WSN;
- Anchor positioning error is considered along with the performance evaluation process. In existing literatures, when assessing positioning accuracy, it is usually assumed that the anchor position is completely accurate and error-free, but under normal circumstances, which is really difficult to satisfy under practical conditions [28]. IMU and TOA techniques also produce many errors due to signal interference and other factors, which result in the uncertainty of the base station location. Therefore, it is also very important to analyze the influence of anchor position errors on the positioning accuracy;
- CRLB and PCRLB are considered when different base station topologies are adopted, as well as compared with commonly used localization algorithms. It further shows that CRLB and PCRLB can be used as reference standards for the improvement of positioning algorithms.

The remainder of this paper is organized as follows. Section 2 presents a preliminary introduction about IMU, TOA and the fusion method. Section 3 gives the error modeling method in proposed IMU/TOA fusion system, from three perspectives including IMU method error, anchor position error, and TOA error. Section 4 deduces the CRLB and PCRLB under the above factors and performs the corresponding experimental verification. Section 5 CRLB and PCRLB are considered when different base station topologies are used, as well as compared with commonly used localization algorithms. Then, conclusions are drawn in Sect. 6.

2 Fusion Positioning Method

2.1 IMU-Based Positioning Method

IMU is a kind of self-contained navigation system, generally including a triaxial accelerometer and a triaxial gyroscope. Accelerometers detect the accelerations of the target in the carrier coordinate system [11]. Gyroscopes detect the angular velocities of the target relative to the navigation coordinate system. By measuring the accelerations and angular velocities of the target in 3-D space, the step length and

direction information are obtained through attitude calculation [29]. According to the step size and direction information, the target position of the next state can be predicted [11, 29].

Supposed carrier coordinate system is b. We denote obtained acceleration parameter as $\boldsymbol{a}_b = [a_{bx}\ a_{by}\ a_{bz}]$, and the gyro parameter as $\boldsymbol{\omega}_b = [\omega_{bx}\ \omega_{by}\ \omega_{bz}]$. Therefore, the motion angles information of the navigation target (namely pitch angle, heading angle and roll angle) are respectively ψ, θ, γ. Thus, the coordinate rotation matrix C_b^t from the carrier coordinate system to the navigation coordinate system is represented as:

$$C_b^t = \begin{bmatrix} cos\gamma cos\psi + sin\gamma sin\psi sin\theta & sin\psi cos\theta & sin\gamma cos\psi - cos\gamma sin\psi sin\theta \\ -cos\gamma cos\psi + sin\gamma sin\psi sin\theta & cos\psi cos\theta & -sin\gamma cos\psi - cos\gamma sin\psi sin\theta \\ -sin\gamma cos\theta & sin\theta & cos\gamma cos\theta \end{bmatrix} \tag{1}$$

Furthermore, subtracted by the acceleration of gravity $\boldsymbol{g} = \begin{bmatrix} 0 \\ 0 \\ g \end{bmatrix}$, we could obtain the instantaneous acceleration value of the carrier at time t in the geographic coordinate system, i.e.,

$$\begin{bmatrix} a'_{tx} \\ a'_{ty} \\ a'_{tz} \end{bmatrix} = C_b^t \begin{bmatrix} a_{tx} \\ a_{ty} \\ a_{tz} \end{bmatrix} - \begin{bmatrix} 0 \\ 0 \\ g \end{bmatrix} \tag{2}$$

Since the sampling interval of IMU is very short, it can be considered that the motion of the carrier is a straight line motion with uniform speed change. Then, the displacement and angle change of moving target can be anyhow calculated [1].

2.2 TOA-Based TOA Positioning Method

TOA is a method of estimating the distance length by measuring the transmission time of wireless signals. The TOA ranging principle is shown in Fig. 1.

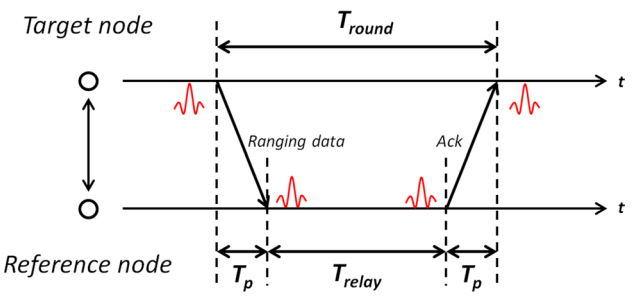

Fig. 1 The principle of TOA ranging

To avoid high accuracy synchronization between target node and reference node, the two-way ranging is the most frequently used method to implement TOA ranging, as shown in Fig. 1. In this algorithm, target node firstly sends out ranging data as an wideband impulse. This impulse will be detected at the reference node and after a period of processing time, the reference node sends back an acknowledgment (Ack) impulse containing the processing time. The round trip flight time between target node and reference node will be recorded upon the arrival of Ack and the target node will calculate the one-way TOA by eliminating the relay period. The distance estimation can be therefore given by:

$$\hat{d} = T_p \times c = \frac{T_{round} - T_{relay}}{2} \times c \tag{3}$$

where T_p represents the single trip propagation time between target node and reference node, T_{relay} denotes to the processing time at the reference node and T_{round} denotes to the round trip propagation time of impulses.

2.3 Fusion Positioning Method

IMU/TOA fusion method can take advantages of their respective strengths to solve the problems of accumulative errors and instantaneous accuracy. Generally, filtering [12, 13] and optimization methods [30] are considered in the fusion of multiple sensors. In this study, we take Kalman filtering [12] as an example, to present the feasibility of fusion methods. More possible algorithms could be referred to [12–15]. Then, fundamental limits are derived to evaluate the performance of IMU/TOA fusion-based localization in WSN.

The Kalman filter algorithm is an estimation method that estimates the state sequence of a dynamic system optimally, and makes the estimated value of the system state have a minimum mean square error [34]. It includes two parts: prediction and update. This paper uses the Kalman filter algorithm to achieve the integration of IMU and TOA multisource data.

Let $\boldsymbol{m_k} = [x_k, y_k, z_k]^T, k = 1, 2, \ldots, K$ denote the state vector of the mobile node in state k, where (x_k, y_k, z_k) denotes the 3-D coordinate of the node in world coordinate space and K denotes the total state observation number. Let $\boldsymbol{z}_k$ denote the measurement vector of the mobile node in state k, then the equation of state and observation equation for the system can be defined as

$$\begin{cases} \boldsymbol{m}_k = A_k \boldsymbol{m}_k + q_k \\ z_k = H_k \boldsymbol{m}_k + r_k \end{cases} \tag{4}$$

where $\boldsymbol{q_k}$ indicates the process error, which is based on the error of the IMU, obeys a Gaussian distribution with a mean of 0 and a covariance of Q. r_k denotes the measurement error, that is, the TOA ranging error, which obeys a Gaussian distribution with a mean of 0 and a covariance of R. Matrix $\boldsymbol{A_k}$ and matrix $\boldsymbol{H_k}$ represent state transition matrix and measurement relation matrix, respectively.

We can use the Kalman filter algorithm to predict the position of the mobile node based on the state equation, and then update the position of the mobile node according to the measurement equation. Let $\overline{\hat{\boldsymbol{m}}}_k$ be a priori estimate of $\boldsymbol{m}_k$, i.e., the predicted value, and let $\hat{\boldsymbol{m}}_k$ denote an unbiased estimate, i.e., an updated value. The prior estimate of the error covariance is $\overline{P}_k = E[(\boldsymbol{m}_k - \overline{\hat{\boldsymbol{m}}}_k)(\boldsymbol{m}_k - \overline{\hat{\boldsymbol{m}}}_k)^T]$ and the posterior estimate is $P_k = E[(\boldsymbol{m}_k - \hat{\boldsymbol{m}}_k)(\boldsymbol{m}_k - \hat{\boldsymbol{m}}_k)^T]$. Kalman filter algorithm is described in Algorithm 1.

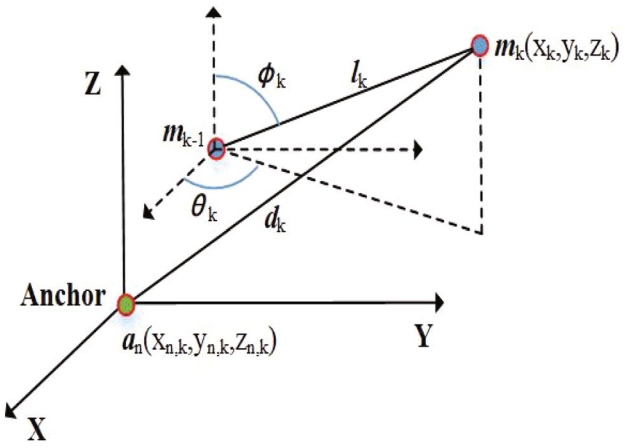

Fig. 2 The state transition of one target node

Thereinto, we can conclude that the sources of error in IMU/TOA fusion positioning methods are: (1) IMU step error and direction error, (2) anchor position error and (3) TOA ranging error.

Algorithm 1 Kalman Filtering Algorithm

Input: : Initialized $\boldsymbol{m}_1$, $\hat{\boldsymbol{m}}_1 = \hat{z}_1$ and $P_1 = E[(\boldsymbol{m}_1 - \hat{\boldsymbol{m}}_1)(\boldsymbol{m}_1 - \hat{\boldsymbol{m}}_1)^T]$.

1: **for** $k = 1, 2, ..., K$ **do**
2: Predict the state, $\overline{\hat{\boldsymbol{m}}}_k = A\hat{\boldsymbol{m}}_{k-1}$
3: Predict state error covariance, $\overline{P}_k = A_k P_{k-1} A_k^T + Q$
4: Compute Kalman gain, $K_k = \overline{P}_k H_k^T (H_k \overline{P}_k H_k^T + R)^{-1}$
5: Update the state, $\hat{\boldsymbol{m}}_k = \overline{\hat{\boldsymbol{m}}}_k + G_k(\boldsymbol{z}_k - H_k \overline{\hat{\boldsymbol{m}}}_k)$
6: Update state error covariance, $P_k = (I - G_k H_k)\overline{P_k}$
7: **end for**

3 Error Modeling

The fusion positioning method based on TOA and IMU will also produce some errors in the positioning process. Since the inertial information used in the attitude calculation process has errors, the obtained step length information and direction information also have errors. TOA-based positioning method knows the location of the base station in advance, but in general, the locations of the base stations are obtained by GPS technology or manual measurements, which are also affected by factors such as noise, resulting in uncertainty of the locations of the base stations, thereby further affecting the positioning accuracy. In addition, when measuring the distance between the target node and the base station, the ranging error may also be caused due to environmental interference and other factors.

Supposed that the coordinate of the target node at the time k is $\boldsymbol{m}_k = [x_k, y_k, z_k]^T$, and the coordinate of the nth base station is $\boldsymbol{a}_n = [x_{n,k}, y_{n,k}, z_{n,k}]^T, n = 1, 2, \ldots, N$, where N is the number of anchor nodes. The schematic diagram of the state of the target node is shown in Fig. 2.

The state information matrix of the target node is $\boldsymbol{m} = [\boldsymbol{m}_1, \boldsymbol{m}_2, \ldots, \boldsymbol{m}_K]^T$ and K is the total state number. For each element in the state information matrix, the following formula can be obtained by

$$\boldsymbol{m}_k = \boldsymbol{m}_{k-1} + l_k \boldsymbol{w}_k + \boldsymbol{r}_k \tag{5}$$

where l_k is the moving step of the node from state $k-1$ to state k, $\boldsymbol{w}_k = [sin\phi_k, cos\theta_k, sin\phi_k sin\theta_k, cos\phi_k]^T$ is the moving direction of the node, $\boldsymbol{r}_k$ the overall error caused by step error and direction error.

3.1 Error Modeling Based on IMU Method

The estimated step size based on IMU can be represented as

$$\hat{l}_k = l_k + u_k, u_k \sim N(0, \sigma_{1,k}^2) \tag{6}$$

where l_k is the actual step size, i.e.,

$$l_k = \sqrt{(x_k - x_{k-1})^2 + (y_k - y_{k-1})^2 + (z_k - z_{k-1})^2} \tag{7}$$

u_k is the step error, which obeys the Gaussian distribution with a mean of 0 and a variance of $\sigma_{1,k}^2$. The estimated vertical angle based on IMU can be represented as

$$\hat{\phi}_k = \phi_k + v_k, v_k \sim N(0, \sigma_{2,k}^2) \tag{8}$$

where ϕ_k is the actual vertical angle, i.e.,

$$\phi_k = arccos\frac{z_k - z_{k-1}}{l_k} \tag{9}$$

where v_k is the vertical angle error, which obeys the Gaussian distribution with a mean of 0 and a variance of $\sigma_{2,k}^2$. The horizontal angle estimate based on the IMU can be expressed as

$$\hat{\theta}_k = \theta_k + \varepsilon_k, \varepsilon_k \sim N(0, \sigma_{3,k}^2) \tag{10}$$

where θ_k is the actual horizontal angle, i.e.,

$$\theta_k = arctan\frac{y_k - y_{k-1}}{x_k - x_{k-1}} \tag{11}$$

ε_k is the horizontal angle error, which obeys the Gaussian distribution with a mean of 0 and a variance of $\sigma_{3,k}^2$.

3.2 Anchor Position Error Modeling

In the first section of this chapter, we define the coordinate of the nth base station as $\boldsymbol{a}_n = [x_{n,k}, y_{n,k}, z_{n,k}]^T, n = 1, 2, \ldots, N$. Supposed that the base station coordinate errors are $\delta_{x_n}, \delta_{y_n}, \delta_{z_n}$, respectively, the actual estimation of the base station coordinate is

$$\begin{aligned}\hat{\boldsymbol{a}}_n =& [\hat{x}_{n,k}, \hat{y}_{n,k}, \hat{z}_{n,k}]^T \\ =& [x_{n,k} - \delta_{x_n}, y_{n,k} - \delta_{y_n}, z_{n,k} - \delta_{z_n}]^T\end{aligned} \tag{12}$$

where $\delta_{x_n}, \delta_{y_n}, \delta_{z_n}$ obey Gaussian distributions with a mean of 0 and a variance of $\sigma_{\delta_{x_n}}, \sigma_{\delta_{y_n}}, \sigma_{\delta_{z_n}}$, respectively.

3.3 Error Modeling Based on TOA Method

The distance between the target node and the anchor node measured by TOA ranging method is estimated as

$$\begin{aligned}\hat{d}_{n,k} &= ||\boldsymbol{m}_k - \hat{\boldsymbol{a}}_n||_2 + e_{1,k} = d_{n,k} + e_{2,k} + e_{1,k} \\ &= d_{n,k} + e_k\end{aligned} \tag{13}$$

where $d_{n,k}$ is the actual distance between the target node and the nth anchor node, i.e.,

$$d_{n,k} = \sqrt{(x_k - x_{n,k})^2 + (y_k - y_{n,k})^2 + (z_k - z_{n,k})^2} \tag{14}$$

where $e_{1,k}$ is the ranging error caused by TOA method, which obeys a Gaussian distribution with a mean of 0 and a variance of $\sigma_{4,k}^2$, i.e., $e_{2,k}$ is the ranging error caused by the anchor position error. Bring Equation (12) and (14) into Equation (13), and ignore the second-order error term, we can get

$$e_{2,k} \approx \frac{(x - x_{n,k})\delta_{x_n} + (y - y_{n,k})\delta_{y_n} + (z - z_{n,k})\delta_{z_n}}{d_{n,k}} \tag{15}$$

We denote $\sigma_{5,k}^2 = \frac{(x-x_{n,k})^2\sigma_{\delta_{x_n}}^2 + (y-y_{n,k})^2\sigma_{\delta_{y_n}}^2 + (z-z_{n,k})^2\sigma_{\delta_{z_n}}^2}{d_{n,k}^2}$. Thus,

$$e_k \sim N(0, \sigma_{4,k}^2 + \sigma_{5,k}^2) \tag{16}$$

4 Positioning Performance Evaluation

In this section, based on above models, CRLB and PCRLB in 3-D environment are deduced to evaluate positioning accuracy in both spatial and temporal level. We define $\nabla_a = [\frac{\partial}{\partial a_1}, \frac{\partial}{\partial a_2}, \ldots, \frac{\partial}{\partial a_M}]^T$ as a gradient vector, define $\Delta_b^a = \nabla_b \nabla_a^T$, define $p(a)$ as the probability density function of the random variable a, and define $tr\{\cdot\}$ as the trace of the matrix.

4.1 Spatial Performance Evaluation

4.1.1 Derivation of CRLB

CRLB is represented as a theoretical lower bound for any unbiased estimation and is widely used to assess localization performance. Thus, we comprehensively derive the CRLB for 3D localization of IMU/TOA fusion method in WSNs to evaluate its spatial performance. Here come some definitions. If $\hat{m}_k$ is an unbiased estimate of m_k, then

$$E\left\{(\hat{\boldsymbol{m}}_k - \boldsymbol{m}_k)^2\right\} \geq CRLB = tr\left\{J^{-1}(\boldsymbol{m}_k)\right\} \tag{17}$$

where $J(\boldsymbol{m}_k)$ is the Fisher Information Matrix (FIM) [28]. Before solving the Fisher information matrix, we need to first define the joint probability density function as

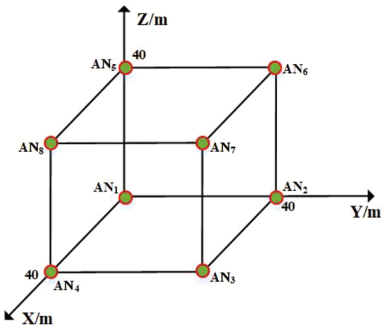

Fig. 3 The deployment of nodes in sensor network

$$p(\hat{d}_k, \hat{l}_k, \hat{\phi}_k, \hat{\theta}_k, \hat{\boldsymbol{m}}_k) = \left\{ \prod_{n=1}^{N} p(\hat{d}_{n,k}|\boldsymbol{m}_k) \right\} p(\hat{l}_k|\boldsymbol{m}_{k-1}, \boldsymbol{m}_k) p(\hat{\phi}_k|\boldsymbol{m}_{k-1}, \boldsymbol{m}_k) p(\hat{\theta}_k|\boldsymbol{m}_{k-1}, \boldsymbol{m}_k) \quad (18)$$

where $p(\hat{l}_k|\boldsymbol{m}_{k-1}, \boldsymbol{m}_k), p(\hat{\phi}_k|\boldsymbol{m}_{k-1}, \boldsymbol{m}_k), p(\hat{\theta}_k|\boldsymbol{m}_{k-1}, \boldsymbol{m}_k)$ and $p(\hat{d}_{n,k}|\boldsymbol{m}_k)$ can be obtained according to Eqs. (5)–(16).

According to the joint probability density function, we can define the FIM as

$$J(\boldsymbol{m}_k)_{i,j} = -E\left[\frac{\partial^2 lnp(\hat{d}_k, \hat{l}_k, \hat{\phi}_k, \hat{\theta}_k, \boldsymbol{m}_k)}{\partial \boldsymbol{m}_{k,i} \partial \boldsymbol{m}_{k,j}} \right], i, j = 1, 2, 3. \quad (19)$$

Bringing Equation (18) into Equation (19), each element of the FIM could be derived, and further obtain CRLB.

4.1.2 Experimental Verification

A stereoscopic sensor network environment is considered like a commercial building, as shown in Fig. 3. Eight anchor nodes are deployed and distributed in each corner of the experiment scenario. Target nodes are distributed in the middle of the area. The dots in Fig. 3 represent anchor nodes. Supposed that the communication range of each anchor may cover the entire area, and anchor nodes can receive the required information from all target nodes. Target nodes are supposed to perform a uniform linear motion along the X direction. The movement speed is $1m\ /\ s$ and the sampling interval is $1s$. Then, $y_k - y_{k-1} = 0m$, $z_k - z_{k-1} = 0m$, and $l_k = ||\boldsymbol{m}_k - \boldsymbol{m}_{k-1}||_2 = 1m$.

CRLB reflects the performance characteristics of tracking nodes in the aspect of relative position distribution. Next, we mainly focus on how well proposed fusion mehtod performs, compared with sole IMU or TOA method.

(1) CRLB of IMU/TOA Fusion and Solo TOA Method

Figure 4a, b respectively show the CRLB of IMU/TOA fusion and solo TOA method in 3-D scene. The effects of anchor position errors on the results are not considered here. Supposed that $\sigma_{1,k} = 0.5m, \sigma_{2,k} = 10°, \sigma_{3,k} = 10°$, and $\sigma_{4,k} = 0.5m$. Comparing Fig. 4a with b, following conclusions could be drawn:

1. In both conditions, CRLB is relatively higher on the outside of the base station, which is because the geometrical position relationship between the base station and the target will affect CRLB. When the target node is on the outside of the topology of the base station, the occlusion of the base station will lead to undetected-path (UDP) [16] error during the signal transmission process. The UDP errors may result in a large localization error and affect the positioning accuracy. Therefore, in the design of 3-D localization applications, we should keep tracking targets as centrally as possible in the middle of the topology, so as to obtain higher positioning results.
2. When IMU/TOA fusion method is applied, the localization lower bound (CRLB) could reach as low as 0.14m,

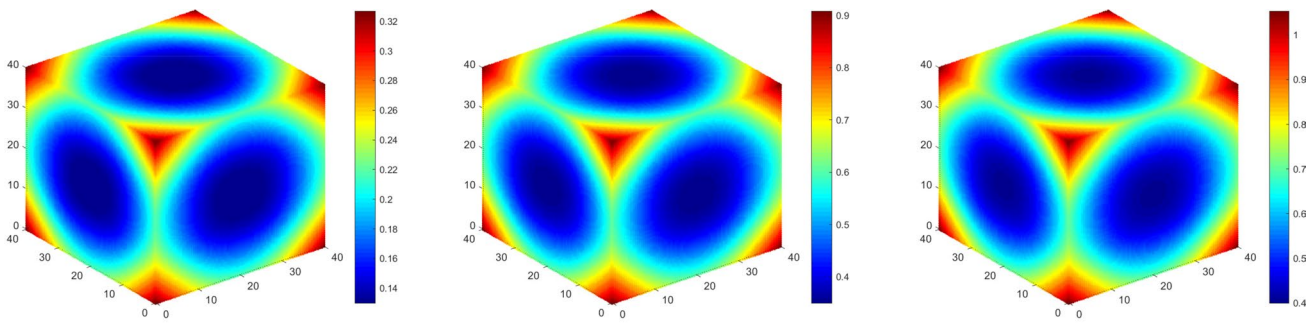

Fig. 4 CRLB with or without considering anchor position error. **a** CRLB of IMU/TOA fusion method without considering anchor position error. **b** CRLB of solo TOA method without considering anchor position. **c** CRLB of IMU/TOA fusion method with considering anchor position error

which is quite better than that of solo TOA method, whose lower bound is 0.4m.

(2) Impact on CRLB with or Without Considering Anchor Position Error

Since the location error of base stations is only considered in TOA ranging, CRLB based on solo TOA method can reflect how base station deployed error contributes to the localization error. The parameters are set as $\sigma_{\delta_{x_n}} = \sigma_{\delta_{y_n}} = \sigma_{\delta_{z_n}} = 0.2m$, and $\sigma_{4,k} = 0.5m$. Figure 4b, c show the impact on the CRLB with or without considering anchor position errors in the case of 3-D localization, respectively. We can draw conclusions that when considering anchor position errors, the positioning accuracy of the system will be reduced by at over 10 cm. It also means that it is necessary to accurately estimate the position of the base station before performing TOA positioning.

4.2 Temporal Performance Evaluation

4.2.1 Derivation of PCRLB

Sequential tracking is supposed to be a temporal problem other than a sole spatial one. These continuous information could be used to evaluate the performance of given algorithms. Thus, we extend the above CRLB to PCRLB with considering posterior information. Before the derivation, we redefine the joint probability density function as

$$\begin{aligned} &p(\hat{d}, \hat{l}, \hat{\phi}, \hat{\theta}, \hat{\boldsymbol{m}}) \\ &= p(\hat{d}_0|\boldsymbol{m}_0) \prod_{k=1}^{K} p(\hat{l}_k|\boldsymbol{m}_{k-1}, \boldsymbol{m}_k) p(\hat{\phi}_k|\boldsymbol{m}_{k-1}, \boldsymbol{m}_k) \\ &\quad p(\hat{\theta}_k|\boldsymbol{m}_{k-1}, \boldsymbol{m}_k) p(\hat{d}_k|\boldsymbol{m}_k) \end{aligned} \tag{20}$$

To calculate FIM at state k, we define

$$p_k = p(\hat{d}_{0:k}, \hat{l}_{0:k}, \hat{\phi}_{0:k}, \hat{\theta}_{0:k}, \hat{\boldsymbol{m}}_{0:k}) \tag{21}$$

where $\hat{d}_{0:k}$, $\hat{l}_{0:k}$, $\hat{\phi}_{0:k}$, $\hat{\theta}_{0:k}$, $\hat{\boldsymbol{m}}_{0:k}$ represent ranging, step length, vertical angle, horizontal angle and target coordinate vector from the start state to state k respectively. Therefore,

$$\begin{aligned} &J(\boldsymbol{m}_{0:k}) \\ &= \begin{bmatrix} E\left\{-\Delta^{\boldsymbol{m}_{0:k-1}}_{\boldsymbol{m}_{0:k-1}} lnp_k\right\} & E\left\{-\Delta^{\boldsymbol{m}_{0:k}}_{\boldsymbol{m}_{0:k-1}} lnp_k\right\} \\ E\left\{-\Delta^{\boldsymbol{m}_{0:k-1}}_{\boldsymbol{m}_{0:k}} lnp_k\right\} & E\left\{-\Delta^{\boldsymbol{m}_{0:k}}_{\boldsymbol{m}_{0:k}} lnp_k\right\} \end{bmatrix} \\ &= \begin{bmatrix} A_k & B_k \\ B_k^T & C_k \end{bmatrix} \end{aligned} \tag{22}$$

According to [37], the sub-matrix J_k can be obtained by pseudo-inverse of the matrix $J(\boldsymbol{m}_{\theta:k})$, i.e.,

$$J_k = C_k - B_k^T A_k^{-1} B_k \tag{23}$$

According to equations (20) and (21), the joint probability density for the $k+1$ state is

$$\begin{aligned} p_{k+1} =& p_k p(\hat{l}_{k+1}|\boldsymbol{m}_k, \boldsymbol{m}_{k+1}) p(\hat{\phi}_{k+1}|\boldsymbol{m}_k, \boldsymbol{m}_{k+1}) \\ & p(\hat{\theta}_{k+1}|\boldsymbol{m}_k, \boldsymbol{m}_{k+1}) p(\hat{d}_{k+1}|\boldsymbol{m}_{k+1}) \end{aligned} \tag{24}$$

According to the joint probability density of state $k+1$, we can find that

$$J(\boldsymbol{m}_{0:k+1}) = \begin{bmatrix} A_k & B_k & 0 \\ B_k^T & C_k + H_k^{11} & H_k^{12} \\ 0 & H_k^{12} & \beta_{k+1} + H_k^{22} \end{bmatrix} \tag{25}$$

where H_k^{11}, H_k^{12}, H_k^{22} reflect the posterior information from state k to state $k+1$, and β_{k+1} reflects the location information based on TOA ranging [36].

From $J(\boldsymbol{m}_{0:k+1})$ and J_k we can get FIM for state $k+1$, i.e.,

$$\begin{aligned} J_{k+1} &= \beta_{k+1} + H_k^{22} - \begin{bmatrix} 0 & H_k^{12} \end{bmatrix} \begin{bmatrix} A_k & B_k \\ B_k^T & C_k + H_k^{11} \end{bmatrix} \begin{bmatrix} 0 \\ H_k^{12} \end{bmatrix} \\ &= \beta_{k+1} + H_k^{22} - H_k^{12} (J_k + H_k^{11})^{-1} H_k^{12} \end{aligned} \tag{26}$$

Due to the step error and the directional error obey Gaussian distribution, $H_k^{11} = H_k^{12} = H_k^{22} = H_k$ can be calculated. The solution of H_k can be referenced [20, 36].

In summary, the posterior FIM is

$$J_{k+1} = \beta_{k+1} + H_k - H_k (J_k + H_k)^{-1} H_k \tag{27}$$

According to the SMW (Sherman–Morrison–Woodbury) formula [38], it can be further simplified as

$$J_{k+1} = \beta_{k+1} + (H_k^{-1} + J_k^{-1})^{-1} \tag{28}$$

where β_{k+1} reflects the information based on TOA, H_k reflects information based on IMU.

4.2.2 Experimental Verification

We use the root mean square of PCRLB to evaluate the performance of the fusion positioning method. The root mean square of the PCRLB can be represented by $\frac{1}{L}\sum_{i=1}^{L} P_k^i$, where P_k^i represents the PCRLB of the mobile node in state k in the ith Monte Carlo experiment, and L represents the total number of Monte Carlo experiments [36]. In this paper, L is taken as 1000. Supposed that the initial position of the mobile node is (1, 1, 1) , and the mobile node performs random motion in the scene to ensure the equilibrium of entire target node's movement process.

Since TOA compensates for the cumulative error of the IMU during the entire motion, it is assumed that the step error and the directional error remain the same throughout the entire motion. The step error measured by the IMU is proportional to the actual step size, i.e., $\sigma_{1,k} = \eta l_k$, where η is the

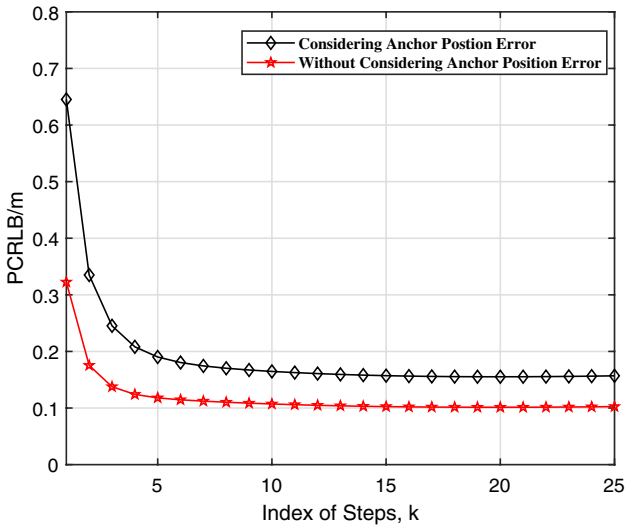

Fig. 5 PCRLB of different positioning methods

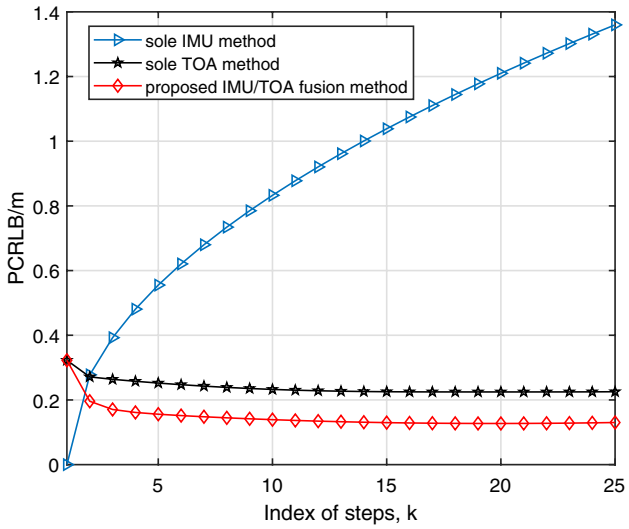

Fig. 6 Effect of anchor position error on PCRLB

proportional coefficient. Assume that $\sigma_{2,k} = 10°$, $\sigma_{3,k} = 10°$, $\sigma_{4,k} = 0.5\,\text{m}$, $\sigma_{\delta_{x_n}} = 0.2\,\text{m}$, $\sigma_{\delta_{y_n}} = 0.2\,\text{m}$, $\sigma_{\delta_{z_n}} = 0.2\,\text{m}$. Random motion is generated by randomly generating 3 directions of velocity, and the sampling interval is 1s.

We mainly analyze the influence of different situations on PCRLB from the following two perspectives. Other comparison results can be found in reference [36].

(1) Impact on PCRLB Based on Different Positioning Methods

Figure 5 shows the theoretical minimum error that can be achieved using the TOA based method alone (i.e., no IMU method), the IMU based method alone (i.e., no TOA ranging method), and IMU/TOA fusion positioning method under a 3-D environment.

It can be seen from Fig. 5 that: (1) Compared with the single TOA based method, the fusion positioning method significantly improves the accuracy of the mobile node. (2) Compared with a single IMU based method, the fusion positioning method compensates for the cumulative error problem based on the IMU method and tends to be stable after a certain time.

1. When only inertial sensors are adopted in the tracking system, as indicated by the black solid line in Fig. 5, the accumulative errors may tend to be diverging. Theoretically, this confirms that IMU based HMT system faces the problem of accumulative errors. However, IMU/TOA fusion method can avoid this divergence. The performance curves of proposed approaches achieve stability after certain steps, i.e., their errors converge.
2. Compared with sole TOA tracking method, IMU/TOA fusion based method can significantly increase the accuracy of human body motion tracking. The lower bound of proposed fusion method could drop below 8 cm.

(2) Impact on PCRLB with or Without Considering Anchor Position Error

Figure 6 shows the PCRLB in the fusion localization method with or without considering anchor position errors. It can be seen from Fig. 6 that the anchor position error will have a certain impact on the positioning accuracy of the system and the accuracy will be reduced by at least 4 cm.

5 Typical Application of Evaluation Methods

CRLB and PCRLB characterizes the lower bound of positioning errors that a localization system can achieve in spatial and temporal level, respectively. They are of great significance in theoretical and practical applications. For example, CRLB can be used to evaluate the performance of base station topology in certain scenarios. Simulation of CRLB could complete the task instead of practical measurements. Both CRLB and PCRLB could be used to verify the localization performance of targeted algorithms [2]. In this section, we will respectively introduce the practical use cases of CRLB and PCRLB in these two aspects.

5.1 Use case 1: Selection of Base Station Topologies

We conduct simulation to verify how number and topologies of base stations impact on the localization accuracy in a given test-field. A 40m $*$ 40m squared field is chosen, and four typical topologies are set as shown in Fig. 7. We

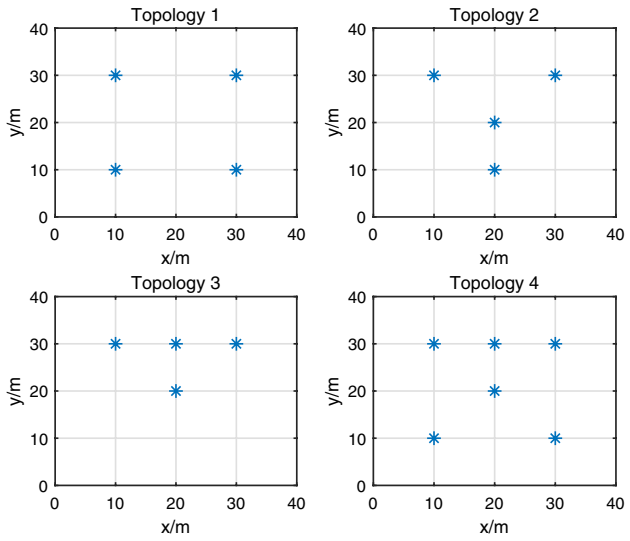

Fig. 7 Different base station topologies

mainly considered how CRLB and PCRLB varies in these different conditions.

5.1.1 Impact on CRLB of Different Base Station Topologies

The variance of TOA ranging is set as $\sigma_{3,k}^2 = 0.5\,\mathrm{m}^2$. Simulation results of CRLB under different topologies are shown in Fig. 8, from which we can draw the following conclusions:

1. When the number of base stations in various topologies are the same, the closer the deployment shape is to a rectangle, the higher the positioning accuracy will be. As shown in Fig. 8a, the deployment shape of the base stations is squared, and the maximum CRLB is around 0.65m, whereas that in Fig. 8b, c are 1.3m and 1.8m, respectively. Thus, differences of 0.65m and 1.15m on positioning accuracy are introduced due to the different base station topologies.

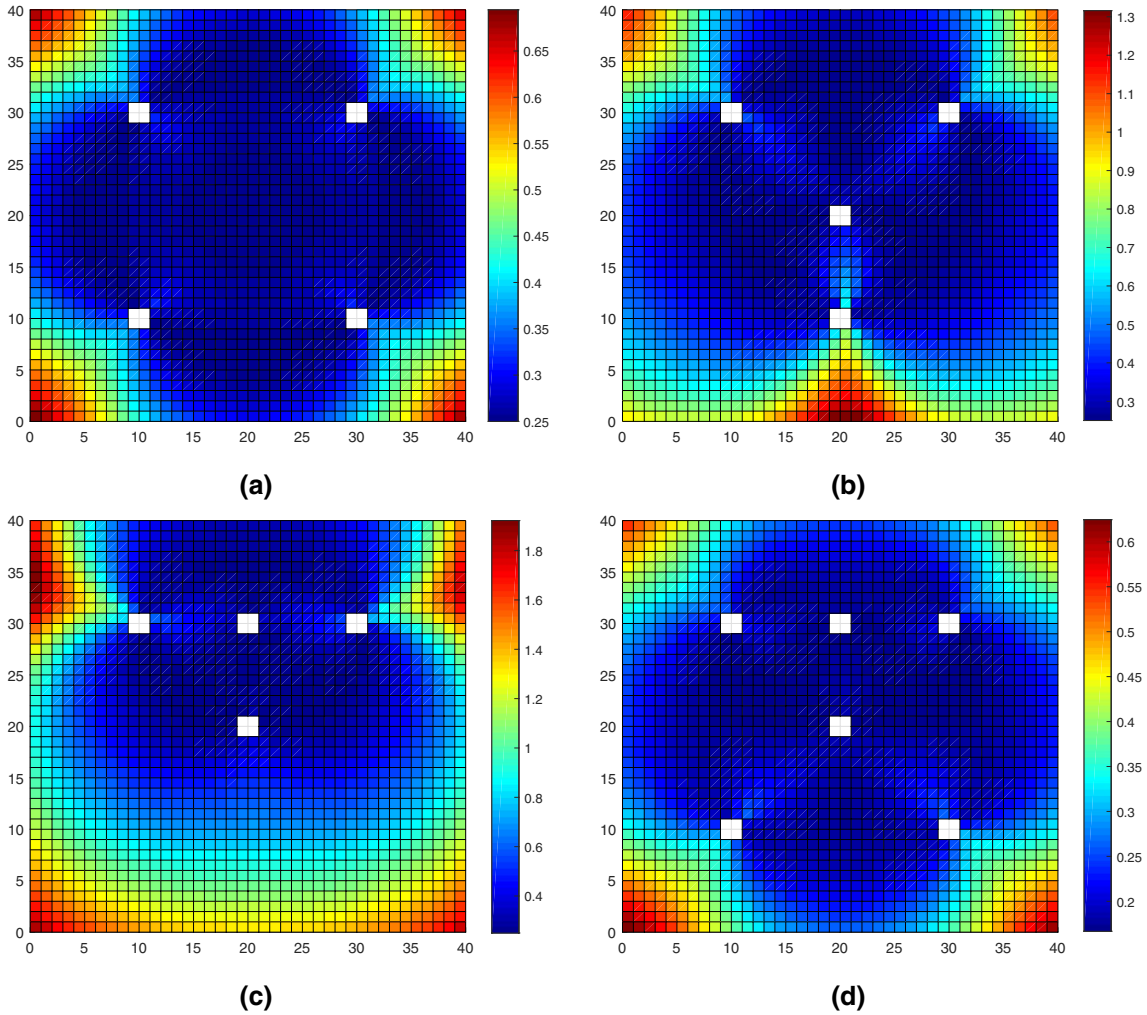

Fig. 8 CRLB under various base station topologies

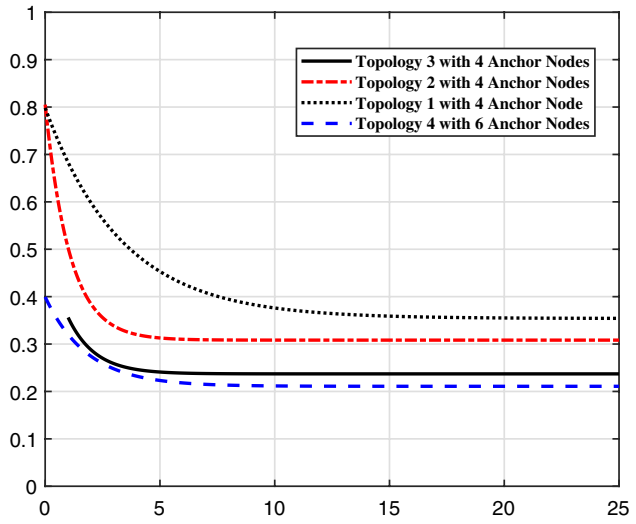

Fig. 9 Impact on PCRLB of different base station topologies

2. Fig. 8c got a highest CRLB among the four, i.e., the worst positioning performance, possibly due to the dense deployment of base stations.
3. In Fig. 8d, a relatively lower CRLB is achieved compared with the other conditions, and around 5cm accuracy improvement is acquired. The denser the base station deployment is, the higher positioning accuracy it may achieve, which is quite consistent with our common sense.
4. With the incrementation of base station numbers, the positioning accuracy increases, but the increase is quite small in contrast to the deployment of base stations. In practical applications, the base station deployment cost is very high, and an extra base station may take lots of human and material resources. Thus, in practical design of fusion positioning systems, more attention should be focused on the optimization of base station topology to obtain higher positioning accuracy.

5.1.2 Impact on PCRLB of Different Base Station Topologies

In terms of PCRLB, the step size of IMU is set as $\alpha = 0.1$, the variance of horizontal angle is $\sigma_2 = 10°$ and that of TOA ranging is $\sigma_{3,k}^2 = 0.5m^2$. From the PCRLB simulation results shown in Fig. 9, following conclusions could be drawn:

1. In condition of the same number of base stations, different topologies lead to various PCRLB accuracy, such as PCRLB of Topology 1 is 0.235 m, that of Topology 2 is 0.305 m, and that of Topology 3 si 0.355 m. Similarly with the CRLB, more uniform topology can obtain better positioning accuracy.

Table 1 Comparison of RMSE For different location algorithms and CRLB

Algorithms	RMSE (without anchor position errors)	RMSE (with anchor position errors)
Centroid	0.6814	0.7725
Least-square	0.6465	0.6639
Taylor series expansion	0.4850	0.5230
IMU/TOA fusion	0.28	0.35
CRLB	0.1128	0.1213

2. Different numbers of base stations have little impact on positioning accuracy. PCRLB of topology 4 is 0.205 m. By comparing Topology 1 and Topology 4, it can be seen that positioning accuracy has been improved by only 3cm.

5.2 Use Case 2: Evaluation on Performance of Algorithms

CRLB reflects the positioning performance of the fusion positioning system in the spatial state, and the positioning algorithm calculates the target position based on the measured values in the spatial state, so the optimal positioning algorithm can be selected by comparing CRLB with RMSE of different positioning algorithms. In addition, CRLB can directly see the difference between the positioning algorithm and the theoretical positioning accuracy. It is used for the later optimization of the positioning algorithm. PCRLB reflects the temporal positioning performance of positioning systems, thus can be used as another criterion for the performance evaluation of the positioning system.

5.2.1 Impact on CRLB of Different Localization Algorithms

Firstly, we mainly verify the three most commonly used positioning algorithms, namely, centroid positioning, least squares positioning, and Taylor series expansion positioning, with proposed IMU/TOA fusion method. Two simulation scenarios are considered, with or without considering anchor position errors.

The result of the positioning algorithm is represented by the root mean square error (RMSE), i.e.,

$$RMSE = \sqrt{\frac{\sum_{i=1}^{n} \varepsilon_i^2}{n}} \tag{29}$$

where ε_i denotes the positioning error at each sample point and n denotes the number of samples. The comparison results are shown in Table 1, from which we could draw the following conclusions:

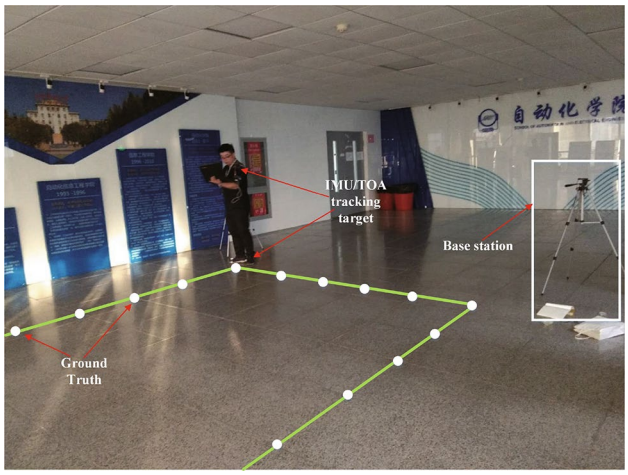

Fig. 10 Schematic diagram of experimental scene setting

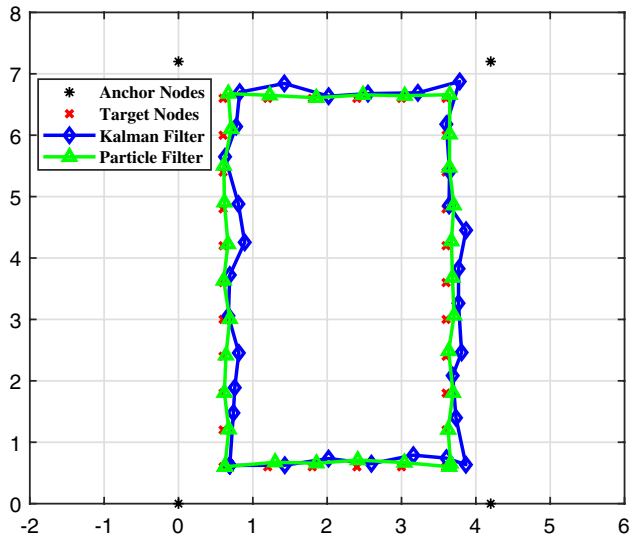

Fig. 11 PCRLB of different positioning methods

1. Under the same experimental conditions, the localization accuracy varies as different algorithms are adopted. IMU/TOA fusion based method shows better positioning accuracy regardless of anchor position errors taken into considerations.
2. Compared with CRLB, all presented methods have large room to be improved. The gap between CRLB and localization results may be caused by sensor accuracy limit or geometric and physical characteristics of the experimental scene. More efforts could be paid to error modeling in practical applications.

5.2.2 Impact on CRLB of Different Filtering Algorithms

In practical positioning systems, such as warehouse robot localization and navigation, the parameter vectors change

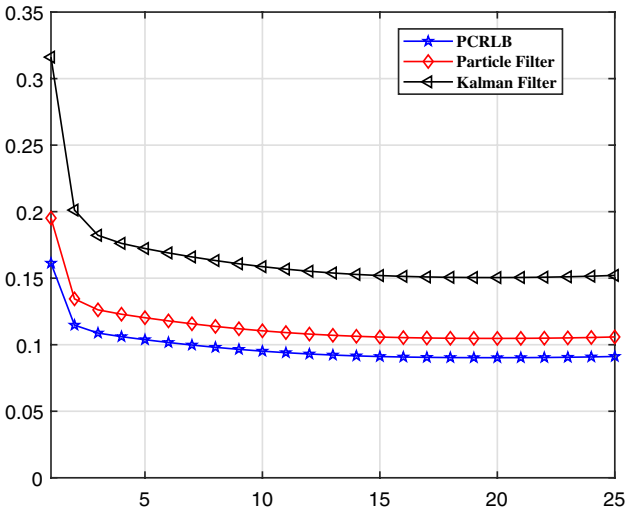

Fig. 12 PCRLB of different positioning methods

over time, so PCRLB needs to be used as a reference for the lower bound estimation. PCRLB is a theoretical analysis tool that is closer to practical application, and can judge whether the parameters of a fusion positioning system have reached the optimal level and whether there is still room for improvement. Therefore, we compared PCRLB with data fusion methods to further verify the theoretical reference values.

As shown in Fig. 10, we set up an experimental scenario of 4.8 m × 7.2 m × 1.5 m, where four anchors are located at each of the corner. Tracking targets are instructed to move following the rectangle line indicated in Fig. 10. Kalman [12] and particle filtering [14] are chosen as methods of comparative experiment, compared with calculated PCRLB. The experiment results are shown in Figs. 11 and 12.

As can be seen from Fig. 11, the estimation result of particle filter algorithm is closer to the ground truth of the target node, while Kalman filter will deviate from the real value at many moments. In order to further evaluate the performance of fusion filtering algorithms, PCRLB was used as a criterion to calculate the root mean square error (RMSE) of various algorithms at different times. The comparison results are shown in Fig. 12.

As can be seen from Fig. 12, (1) Kalman filtering algorithm deviates greatly from PCRLB, while the mean square error of particle filtering algorithm is closer to PCRLB. It is possibly because particle filtering algorithm is not limited by gaussian error hypothesis, and also has the characteristics of high computational efficiency and easy implementation. (2) Particle filtering algorithm still has many shortcomings compared with PCRLB due to particle degradation, particle sample shortage and other problems. Thus, it can be considered to combine other fusion algorithms to improve performance.

6 Conclusion

This paper presents a comprehensive study on the performance evaluation of IMU/TOA fusion method for localization in wireless sensor networks. IMU/TOA fusion can improve the positioning accuracy with compensating TOA multipath effects and overcoming the error accumulation problems of IMU. In order to evaluate the positioning accuracy under real-world conditions, anchor position error, IMU error and TOA error are modeled. Based on these models, CRLB and PCRLB in 3-D environment are deduced to evaluate positioning accuracy in both spatial and temporal level. Finally, CRLB and PCRLB are considered when different base station topologies are used, as well as compared with commonly used localization algorithms. Experimental results show that the effect of anchor position error on positioning results cannot be ignored. CRLB and PCRLB can be used as benchmarks based on IMU/TOA fusion positioning systems and as reference lower bounds for performance improvement for localization algorithms.

Acknowledgements This work is supported by The National Key R&D Program of China, No. 2018YFB0704301, National Natural Science Foundation of China (NSFC) Project Nos. 61671056, 61302065, 61304257, 61402033, Beijing Natural Science Foundation Project No.4152036 and Tianjin Special Program for Science and Technology No. 16ZXCXSF00150.

References

1. J. Rantakokko, J. Rydell, P. Strömbäck, et al., Accurate and reliable soldier and first responder indoor positioning: multisensor systems and cooperative localization, *IEEE Wireless Communications*, Vol. 18, No. 2, pp. 10–18, 2011.
2. S. R. Gandhi, A. Ganz and G. Mullett, FIREGUIDE: Firefighter guide and tracker. Engineering in Medicine and Biology Society (EMBC), *Annual International Conference of the IEEE, IEEE*, Vol. 2010, pp. 2037–2040, 2010.
3. C. Xu, D. Chai, J. He, et al., InnoHAR: a deep neural network for complex human activity recognition, *IEEE Access*, Vol. 7, pp. 9893–9902, 2019.
4. P. Y. W. Dan, A review: wireless sensor networks localization, *Journal of Electronic Measurement and Instrument*, Vol. 5, p. 000, 2011.
5. J. B. Zhang, P. ZHANG and K. DU, Wireless sensor networks time synchronization based on GPS, *Transducer and Microsystem Technologies*, Vol. 28, pp. 31–33, 2009.
6. S. Yuan and M. Z. Win, Fundamental limits of wideband localization– Part I: A general framework, *IEEE Transactions on Information Theory*, Vol. 56, No. 10, pp. 4956–4980, 2010.
7. R. J. Fontana, Recent system applications of short-pulse ultra-wideband (UWB) technology, *IEEE Transactions on Microwave Theory and Techniques*, Vol. 52, No. 9, pp. 2087–2104, 2004.
8. S. Lee, B. Kim, H. Kim, et al., Inertial sensor-based indoor pedestrian localization with minimum 802.15. 4a configuration, *IEEE Transactions on Industrial Informatics*, Vol. 7, No. 3, pp. 455–466, 2011.
9. C. Xu, J. He, X. Zhang, et al., Geometrical kinematic modeling on human motion using method of multi-sensor fusion, *Information Fusion*, Vol. 41, pp. 243–254, 2018.
10. M. Cornacchia, K. Ozcan, Y. Zheng, et al., A survey on activity detection and classification using wearable sensors, *IEEE Sensors Journal*, Vol. 17, No. 2, pp. 386–403, 2017.
11. S. D. Bao, X. L. Meng, W. Xiao, et al., Fusion of inertial/magnetic sensor measurements and map information for pedestrian tracking, *Sensors*, Vol. 17, No. 2, p. 340, 2017.
12. S. Zhao, Y. S. Shmaliy, P. Shi, et al., Fusion Kalman/UFIR filter for state estimation with uncertain parameters and noise statistics, *IEEE Transactions on Industrial Electronics*, Vol. 64, No. 4, pp. 3075–3083, 2017.
13. D. Briese, H. Kunze and G. Rose, UWB localization using adaptive covariance Kalman Filter based on sensor fusion. Ubiquitous Wireless Broadband (ICUWB), *IEEE 17th International Conference on IEEE*, pp. 1–7, 2017.
14. H. Kim, B. Liu, C. Y. Goh, et al., Robust vehicle localization using entropy-weighted particle filter-based data fusion of vertical and road intensity information for a large scale urban area, *IEEE Robotics and Automation Letters*, Vol. 2, No. 3, pp. 1518–1524, 2017.
15. Z. Liu, L. Zhang, Q. Liu, et al., Fusion of magnetic and visual sensors for indoor localization: infrastructure-free and more effective, *IEEE Transactions on Multimedia*, Vol. 19, No. 4, pp. 874–888, 2017.
16. C. Xu, J. He, X. Zhang, et al., Toward near-ground localization: modeling and applications for TOA ranging error, *IEEE Transactions on Antennas and Propagation*, Vol. 65, No. 10, pp. 5658–5662, 2017.
17. D. Dardari, C. C. Chong and M. Z. Win, Improved lower bounds on time-of-arrival estimation error in realistic UWB channels. In *IEEE International Conference on Ultra-wideband, IEEE*, pp. 531–537, 2006.
18. L. Cong and W. Zhuang, Non-line-of-sight error mitigation in TDOA mobile location. In *Global Telecommunications Conference, 2001. GLOBECOM'01, IEEE*. IEEE, Vol. 1, pp. 680–684, 2001.
19. K. C. Ho and Y. T. Chan, Solution and performance analysis of geolocation by TDOA, *IEEE Transactions on Aerospace and Electronic Systems*, Vol. 29, No. 4, pp. 1311–1322, 1993.
20. C. Xu, J. He, X. Zhang, et al., Towards human motion tracking: multi-sensory IMU/TOA fusion method and fundamental limits, *Electronics*, Vol. 8, No. 2, p. 142, 2019.
21. S. Venkatraman and J. Caffery, Hybrid TOA/AOA techniques for mobile location in non-line-of-sight environments. In *IEEE Wireless Communications and Networking Conference, 2004, WCNC*. IEEE, Vol. 1, pp. 274–278, 2004.
22. C. Zhong, J. Eliasson, H. Makitaavola, et al., A cluster-based localization method using RSSI for heterogeneous wireless sensor networks. In *2010 6th International Conference on Wireless Communications Networking and Mobile Computing (WiCOM) IEEE*, pp. 1–16, 2010.
23. N. Patwari and A O. Hero III, Using proximity and quantized RSS for sensor localization in wireless networks. In *Proceedings of the 2nd ACM international conference on Wireless sensor networks and applications*. ACM, pp. 20–29, 2003.
24. P. H. Tseng and K. T. Feng, Derivation of CRLB for linear least square estimator in wireless location systems, *Wireless Networks*, Vol. 18, No. 7, pp. 735–747, 2012.
25. H. A. Shaban, M. A. El-Nasr and R. M. Buehrer, Toward a highly accurate ambulatory system for clinical gait analysis via UWB radios, *IEEE Transactions on Information Technology in Biomedicine*, Vol. 14, No. 2, pp. 284–291, 2010.
26. Y. Zhang, Y. Zhu and L. Shen, A Semidefinite Relaxation Approach to Positioning in Hybrid Sensor Networks. *IEEE 83rd*

Vehicular Technology Conference (VTC Spring). IEEE, pp. 1–5, 2016.
27. Z. He, Y. Ma and R. Tafazolli, Posterior Cramér-Rao bound for inertial sensors enhanced mobile positioning under the random walk motion model, *IEEE Wireless Communications Letters*, Vol. 1, No. 6, pp. 629–632, 2012.
28. K. Yu, 3-D localization error analysis in wireless networks. *IEEE Transactions on Wireless Communications*, Vol. 6, No. 10, 2007.
29. R. H. Zhang, H. G. Jia, T. Chen, et al., Attitude solution for strap-down inertial navigation system based on quaternion algorithm, *Optics and Precision Engineering*, Vol. 16, No. 10, pp. 1963–1970, 2008.
30. L. Dong, W. Shu, G. Han, et al., A multi-step source localization method with narrowing velocity interval of cyber-physical systems in buildings. *IEEE Access*, Vol. PP, No. 99, p. 1, 2017.
31. B. Zhang, T. Liu, Y. Han, et al., 3-Dimension location algorithm research based on TOA, *Computer Engineering and Design*, Vol. 14, p. 026, 2007.
32. I. Guvenc and C. C.Chong, A survey on TOA based wireless localization and NLOS mitigation techniques. *IEEE Communications Surveys & Tutorials*, Vol. 11, No. 3, 2009.
33. H. Chen, P. Huang, M. Martins et al., Novel centroid localization algorithm for three-dimensional wireless sensor networks. *4th International Conference on Wireless Communications, Networking and Mobile Computing, WiCOM'08*. IEEE, pp. 1–4, 2008.
34. A. Benini, A. Mancini, A. Marinelli, et al., A biased extended kalman filter for indoor localization of a mobile agent using low-cost imu and uwb wireless sensor network[J], *IFAC Proceedings Volumes*, Vol. 45, No. 22, pp. 735–740, 2012.
35. R. Balan, The Fisher information matrix and the CRLB in a non-AWGN model for the phase retrieval problem. In *2015 International Conference on Sampling Theory and Applications (SampTA)*. IEEE, pp. 178-182, 2015.
36. Z. Zeng, S. Liu and L. Wang, UWB/IMU integration approach with NLOS identification and mitigation. In *2018 52nd Annual Conference on Information Sciences and Systems (CISS)*. IEEE, pp. 1–6, 2018.
37. P. Tichavsky, C. H. Muravchik and A. Nehorai, Posterior Cramer-Rao bounds for discrete-time nonlinear filtering, *IEEE Transactions on Signal Processing*, Vol. 46, No. 5, pp. 1386–1396, 1998.
38. C. Y. Deng, A generalization of the Sherman–Morrison–Woodbury formula, *Applied Mathematics Letters*, Vol. 24, No. 9, pp. 1561–1564, 2011.

Cheng Xu received the B.E. and M.S. degree from the University of Science and Technology Beijing (USTB), China in 2012 and 2015, respectively. He is currently working towards the Ph.D. degree in the Data and Cyber-Physical System Lab (DCPS) at University of Science and Technology Beijing. His research interests include patter recognition and internet of things. He is a student member of the IEEE and CCF.

Jie He received B.E. and Ph.D. degree in computer scienece from University of Science and Technology Beijing (USTB), China in 2005 and 2012, respectively. Since July 2015, he has been an associate professor with the School of Computer and Communication Engineering, USTB since 2015. From April 2011 to April 2012, he was a visiting Ph.D. student in Center for Wireless Information Network Studies, Worcester Polytechnic Institute. His research interests includes wireless indoor positioning, human gesture recognition and motion capture.

Xiaotong Zhang received the M.S., and Ph.D. degrees from University of Science and Technology Beijing, in 1997, and 2000, respectively. He was a Professor in the Department of Computer Science and Technology, University of Science and Technology Beijing. His research includes work in quality of wireless channels and networks, wireless sensor networks, networks management, cross-layer design and resource allocation of broadband and wireless network, signal processing of communication and computer architecture.

Shihong Duan received Ph.D. degree in computer scienece from University of Science and Technology Beijing (USTB). She is an associate professor with the School of Computer and Communication Engineering, USTB. Her research interests includes wireless indoor positioning, human gesture recognition and motion capture.

Cui Yao received the B.E. degrees from the University of Science and Technology Beijing, Beijing, China, in 2016 and she is currently working toward the Master degree at University of Science and Technology Beijing. Her research interests include patter recognition and internet of things.